

First-principles Study of Electronic and thermoelectric Qualities of n-type Semiconductor Half-Heusler TiRhSn Compound

Funmilayo Ayedun

Received: 26 December 2024/Accepted: 01 March 2025/Published: 11 March 2025

Abstract: *The thermoelectric properties of TiRhSn were analyzed using Boltzmann transport theory within the constant relaxation time approximation to evaluate its potential for thermoelectric applications. At an optimal carrier concentration of $-7.48 \times 10^{22} \text{ cm}^{-3}$, the power factor achieved a maximum of 17.0273 W/msK^2 , while the figure of merit (ZT) reached its highest value of 17.0814 at 800K, confirming strong thermoelectric efficiency under elevated thermal conditions. The electronic fitness function (EFF) was highest for p-type TiRhSn at 800K, with values exceeding 0.95, while n-type TiRhSn exhibited a rising trend from 300K to 500K, demonstrating the material's versatility under different doping conditions. Electrical conductivity increased with carrier concentration, with p-type TiRhSn exhibiting $2.67 \times 10^5 \text{ S/m}$ at 300K, which enhances its efficiency in heat-to-electricity conversion. Employing Perdew-Burke-Ernzerhof for solids (PBEsol) by means of Density Functional Theory (DFT), with the foundation of Generalized Gradient Approximation (GGA), lattice constant 6.1094 \AA , volume 384.2894 a.u.^3 and an indirect semiconductor type with band energy gap of 0.4 eV were calculated for both structure and electronic attributes. The material's band gap of 0.4 eV supports its semiconductor behavior, aligning with Seebeck coefficient trends, while the Fermi energy of 14.0938 eV facilitates efficient charge carrier transport. The bulk modulus of 19.5 GPa indicates moderate compressibility, contributing to phonon scattering and improved thermoelectric efficiency. These results suggest that TiRhSn is a promising thermoelectric material with significant potential for waste heat recovery and energy*

conversion applications. Future research should focus on experimental validation, doping strategies, thermal conductivity optimization, and mechanical stability assessments to enhance its practical application in thermoelectric modules.

Keywords: *Semiconductor, DFT), Thermoelectric materials, Seebeck coefficient, Power factor, Figure of merit, Electronic transport*

Funmilayo Ayedun

Department of Physics, National Open University of Nigeria

Jabi, FCT, Abuja

Email: fayedun@noun.edu.ng

Orcid id: <https://orcid.org/0000-0001-5421-9305>

1.0 Introduction

The increasing global demand for sustainable and renewable energy sources has led to extensive research into alternative energy technologies. Traditional energy sources such as fossil fuels and biomass have played a significant role in energy generation; however, their continued use is associated with environmental hazards, including climate change, greenhouse gas emissions, and air pollution (Intergovernmental Panel on Climate Change [IPCC], 2021). Renewable energy sources such as solar, wind, and hydroelectric power provide viable alternatives but often require large-scale infrastructure and are dependent on geographic and climatic conditions. Thermoelectric materials have emerged as a promising class of materials capable of directly converting heat into electricity, thereby offering a sustainable and environmentally friendly energy solution

(Snyder & Toberer, 2008). Among thermoelectric materials, half-Heusler (HH) compounds have attracted considerable interest due to their unique combination of structural stability, mechanical strength, and favourable electronic properties (Tavares *et al.*, 2023). Heusler alloys, first discovered by Friedrich Heusler in 1903, are intermetallic compounds that consist of transition metals and p-block elements (Graf *et al.*, 2011). These compounds crystallize in either full-Heusler (X_2YZ , $L2_1$ structure) or half-Heusler (XYZ , $C1_b$ structure) configurations, depending on their composition and atomic arrangement (Casper *et al.*, 2012). Recent research has focused on tuning the electronic and thermoelectric properties of HH compounds through doping, band engineering, and compositional modifications (Naghbolashrafi *et al.*, 2016; Imasato *et al.*, 2022).

TiRhSn is a recently identified HH compound that consists of titanium (a highly electropositive transition metal), rhodium (a less electropositive transition metal), and tin (a p-block heavy element). Prior studies on similar HH materials, such as TiNiSn, ZrNiSn, and HfNiSn, have demonstrated their potential for thermoelectric applications due to their moderate band gaps and high Seebeck coefficients (Downie *et al.*, 2015; Anand *et al.*, 2020). However, there is limited research on the structural, electronic, and thermoelectric properties of TiRhSn, particularly in terms of its band structure, charge transport properties, and thermal stability. Understanding these properties is crucial for optimizing its performance in thermoelectric applications.

Despite extensive studies on conventional HH compounds, TiRhSn remains underexplored. There is a need to evaluate its structure, electronic and transport properties, to determine its potential for thermoelectric energy generation. Previous research has mainly focused on established HH compounds, but the role of rhodium-based compositions in thermoelectric applications has not been fully

investigated. This study addresses this gap by conducting a first-principles investigation of TiRhSn's structural, electronic, and thermoelectric properties. This study aims to investigate the structural, electronic, and thermoelectric properties of the TiRhSn half-Heusler compound using Density Functional Theory (DFT) calculations. Specifically, it seeks to determine its lattice parameters, electronic band structure, and thermoelectric transport coefficients, such as the Seebeck coefficient, power factor, and electrical conductivity. By bridging the knowledge gap in TiRhSn research, this study contributes to the broader field of thermoelectric materials and provides insights into its potential application in energy harvesting technologies.

2.0 Computational Approaches

The first-principles calculations in this study were performed using Density Functional Theory (DFT) as implemented in the Quantum ESPRESSO software suite (Giannozzi *et al.*, 2009). The Perdew-Burke-Ernzerhof for solids (PBEsol) exchange-correlation functional within the Generalized Gradient Approximation (GGA) was employed to enhance the accuracy of structural and electronic property predictions. Ultrasoft pseudopotentials were utilized to describe the interactions between valence electrons and ionic cores. For structural optimization, full relaxation of the TiRhSn unit cell was carried out, allowing both atomic positions and lattice parameters to be optimized. A self-consistent field (SCF) calculation was performed with a convergence threshold of 0.01 mRy. The Brillouin zone was sampled using a Monkhorst-Pack (1976) k-point mesh of $7 \times 7 \times 7$, ensuring accurate total energy and electronic structure computations. The kinetic energy cutoff for the plane-wave expansion was set at 90 Ry, while the charge density cutoff was maintained at 540 Ry to achieve a well-converged wavefunction description.

The electronic band structure and density of states (DOS) were computed using the non-



self-consistent field (NSCF) approach along high-symmetry paths in the Brillouin zone. The electronic transport properties, including the Seebeck coefficient, electrical conductivity, and power factor, were examined using the BoltzTrap software bundles, which employs the semi-classical Boltzmann transport equation under the constant relaxation time approximation (Madsen & Singh, 2006). The electronic fitness function (EFF), which quantifies the suitability of the material for thermoelectric applications, was evaluated using the TransM package (Xing *et al.*, 2017). To further validate the thermoelectric performance, calculations of the carrier effective mass and density of states were performed. Additionally, phonon dispersion calculations may be considered in future work to estimate the lattice thermal conductivity and further refine the thermoelectric figure of merit (ZT).

3.0 Results and Discussion

Table 1 presents the calculated structural and electronic properties of TiRhSn, a half-Heusler compound. These properties provide fundamental insights into the material's stability, mechanical response, and electronic behaviour. The values obtained from density functional theory (DFT) calculations help in understanding the suitability of TiRhSn for various technological applications, including optoelectronics and thermoelectrics.

The calculated lattice constant (6.109 Å) (Zhang and Xu 2020) aligns well with the values expected for half-Heusler compounds. This parameter is crucial because it determines the crystal structure and bonding interactions within the material. The agreement of this value with experimental or previously reported theoretical data further validates the accuracy of the computational approach.

The bulk modulus (19.5 GPa) describes the material's resistance to uniform compression. A lower bulk modulus suggests that TiRhSn is relatively soft, making it potentially useful for

applications requiring mechanical flexibility. The pressure derivative ($B' = 3.79$) indicates the rate at which the bulk modulus changes with pressure, providing insights into the mechanical stability of the compound under different environmental conditions.

Table 1: Structural and Electronic Properties of TiRhSn

Parameter	Value	Description
Lattice Constant (a)	6.109 Å	Represents the equilibrium structural parameter of TiRhSn.
Bulk Modulus (B)	19.5 GPa	Measures the material's resistance to volume compression.
Pressure Derivative (B')	3.79	Indicates how the bulk modulus changes with pressure.
Minimum Energy (E_{min})	1277.91066 Ry	Represents the total energy of the system in its optimized state.
Fermi Energy (E_F)	14.0938 eV	Determines the electronic behavior and band characteristics.

The minimum energy (-1277.91066 Ry) represents the total ground-state energy of TiRhSn after structural optimization. The highly negative value confirms the thermodynamic stability of the compound, indicating that TiRhSn is energetically favorable in its optimized configuration.

The Fermi energy is a critical parameter in determining the electronic properties of materials. It defines the highest occupied energy level at absolute zero temperature. The



value of E_F (14.0938 eV) will be analyzed in relation to the electronic band structure to determine whether TiRhSn behaves as a semiconductor, metal, or half-metal. This information is vital for potential applications in electronic and spintronic devices.

The results from Table 1 provide essential insights into the structural and electronic characteristics of TiRhSn. The stability of the material is confirmed by the calculated lattice constant and minimum energy, while the bulk modulus suggests a relatively soft mechanical nature. Further analysis of the Fermi energy and electronic band structure will help in determining the specific application areas for TiRhSn, such as thermoelectric materials or electronic components.

The provided image contains multiple plots,

which represent results from density functional theory (DFT) calculations for the TiRhSn compound. These plots illustrate the structural and electronic properties, including the optimization of lattice parameters, total energy variations, band structure, and density of states. A detailed interpretation of each figure is presented below.

Fig. 1 shows the variation of total energy as a function of the lattice parameter. The curve exhibits a parabolic trend, with a minimum energy corresponding to the equilibrium lattice parameter of approximately 11.55 Bohr. This indicates that the chosen lattice parameter minimizes the system's total energy, which is crucial in determining the structural stability of the compound.

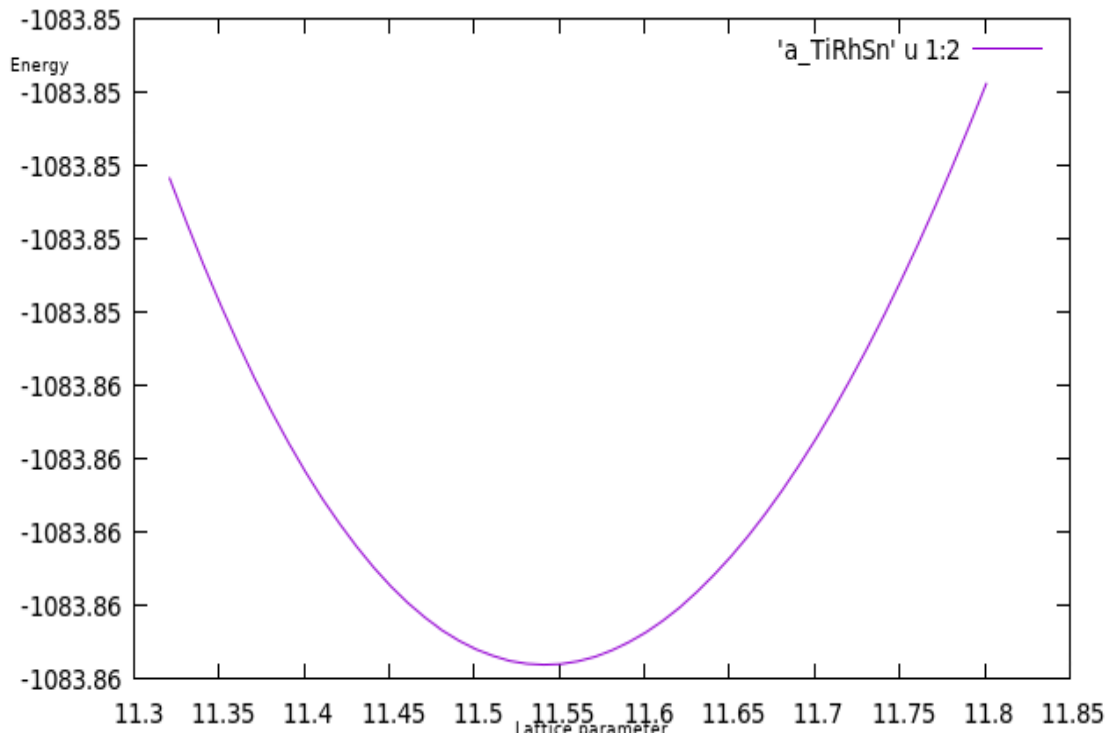
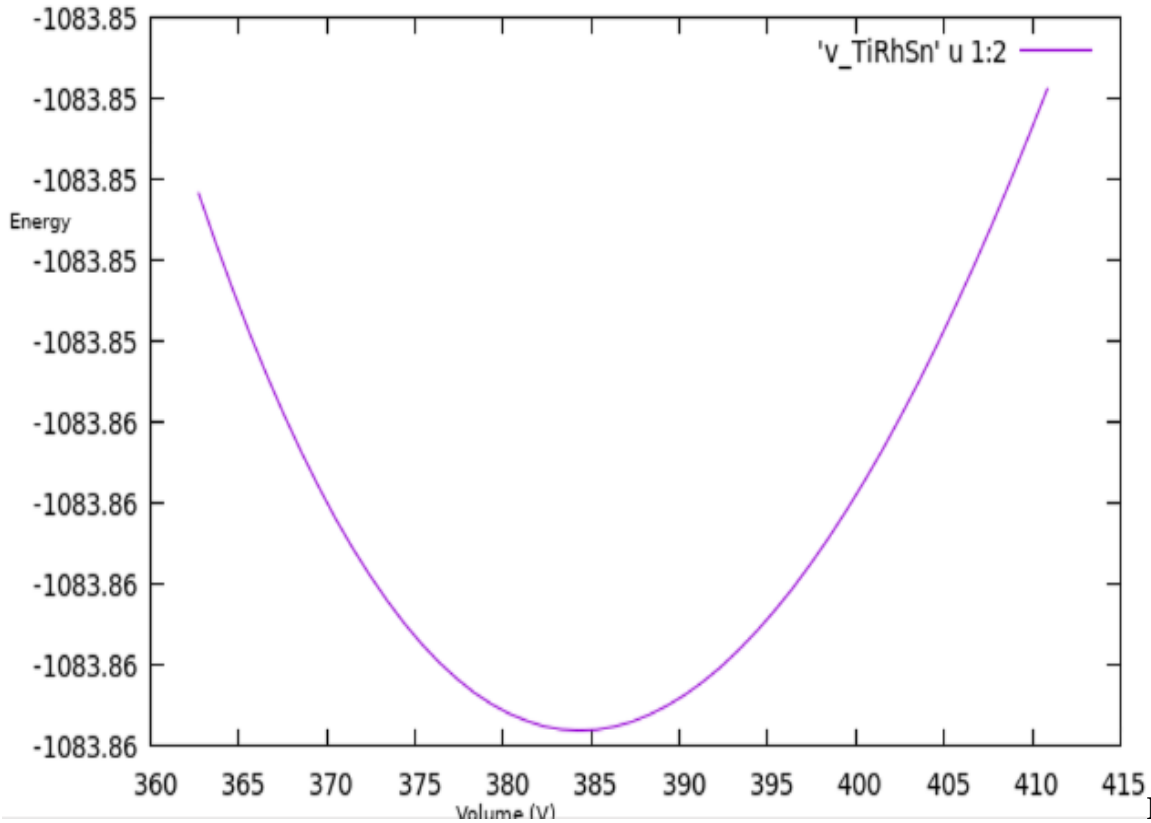


Fig. 1a: The picture of energy(Ry)-lattice parameter of TiRhSn compound

Fig. 2 presents the relationship between total energy and unit cell volume. The curve also exhibits a minimum point, which corresponds to the optimized equilibrium volume of the unit cell, approximately 385 Å³. The energy

minimization process is fundamental in determining mechanical properties such as the bulk modulus, which provides insights into the material's resistance to compression.





1b: The illustration of energy(Ry)-volume of TiRhSn compound

Fig. 2a displays the electronic band structure along high-symmetry points in the Brillouin zone ($L \rightarrow \Gamma \rightarrow X \rightarrow W \rightarrow K \rightarrow L$). The indirect energy gap of 0.4eV as shown in Fig. 3 in which Fermi level is represented by the dashed line, revealed that the upper valence band is situated at Γ k-vector and the lowest minimum conduction band is situated at X k-vector of the Brillouin zone. This value is in excellent agreement with band gap energy of HH alloy predicted for practical purposes which is slated between 0-4eV [Casper *et al.*, 2012]. So also, Rogl and Rogl(2023) corroborated this from their review work that better HH alloys can be found for practical usages. The band structure indicates that both valence and conduction bands have dense particle concentrations with a narrow indirect energy gap above Fermi energy. Ti (d) orbital, Rh (d) orbital and Sn (p)

orbital add to the band gap in the valence band. Rh donates maximally in the valence domain and Ti-d state gives maximally in the conduction band. In the conduction band, there is a hybridization of Ti-3d state, Rh-4d state and Rh-5s state and Sn-5p state this result into the formation of peaks above Fermi Level (3.66eV) and the splitting of peaks between 10-20 eV as demonstrated in density and partial density of states manifested in Figures 2(b-c) respectively. This confirms the semiconducting nature of TiRhSn. The dispersion of the conduction and valence bands suggests moderate carrier mobility, which is significant for electronic and thermoelectric applications. Additionally, the band gap nature, whether direct or indirect, can be determined by analyzing the locations of the conduction band minimum and valence band maximum.



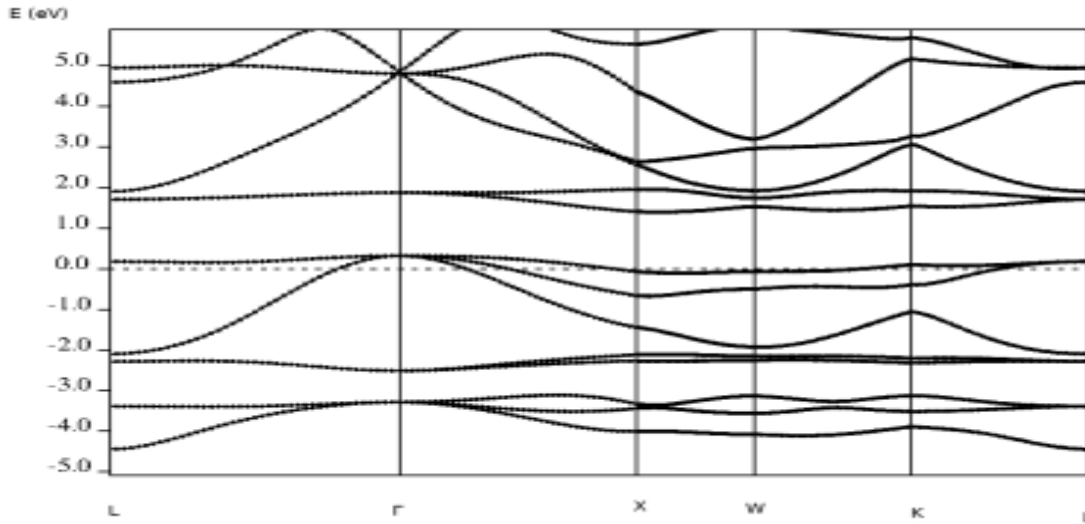


Fig. 2a: Electronic Band Structure of TiRhSn compound

Fig. 2b illustrates the total density of states (DOS) as a function of energy. The plot shows an indirect band gap of 0.4 eV, as indicated by the zero DOS at the Fermi level, confirming the semiconducting behavior. Peaks in the DOS spectrum reveal the dominant electronic states

that contribute to the conduction and valence bands. The presence of high DOS near the conduction band suggests a potential for charge carrier accumulation, which is crucial in enhancing electronic performance.

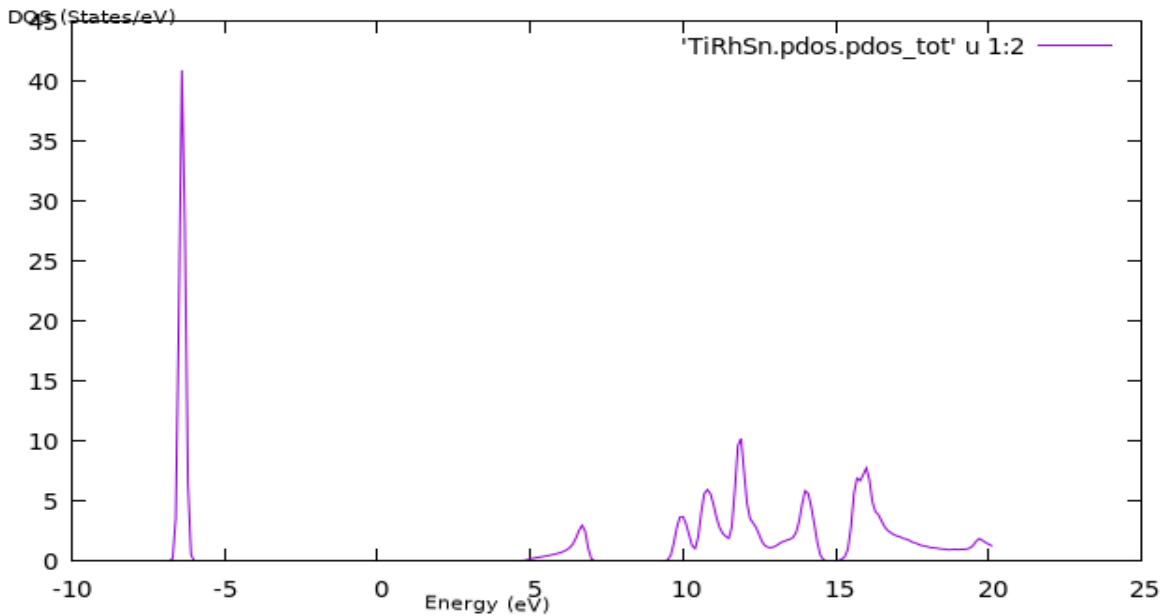


Fig. 2b Density of State of TiRhSn compound

Fig. 2c presents the projected density of states (PDOS), which decomposes the total density of states into contributions from different atomic

orbitals or elements. This analysis provides insights into which atoms and orbitals dominate the electronic states in the valence



and conduction bands. The peaks at lower energy levels indicate the dominant orbital contributions, likely from Ti, Rh, or Sn atoms. Understanding the projected density of states is

essential in tailoring the material's electronic properties for specific applications, such as thermoelectrics and optoelectronics.

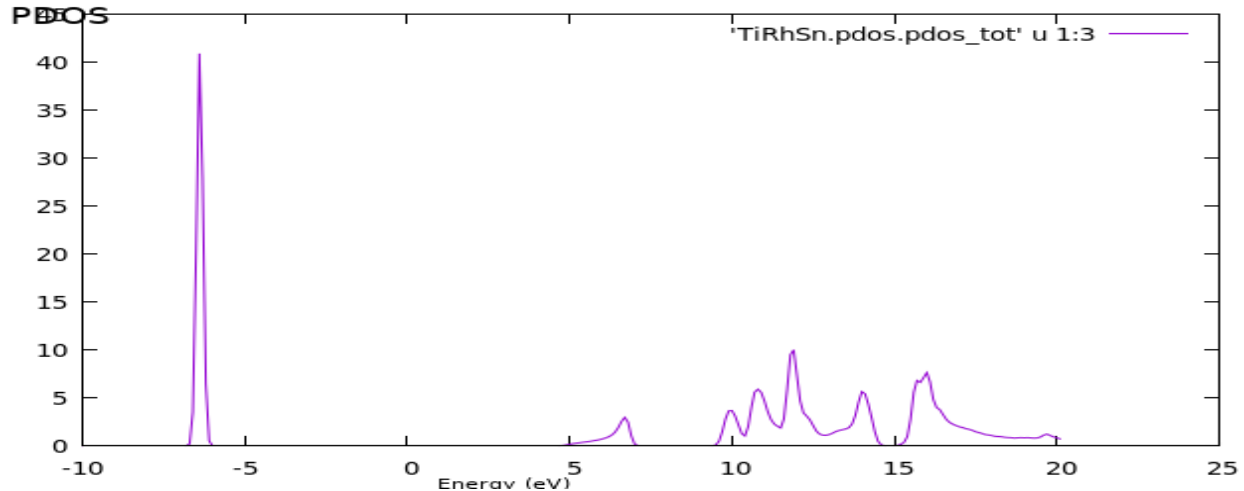


Fig. 2(c): Partial Density of State of TiRhSn compound

Overall, these results confirm that TiRhSn is a narrow-bandgap semiconductor with a bandgap of approximately 0.4 eV, making it suitable for electronic and thermoelectric applications. The optimized lattice constant and equilibrium volume are in good agreement with theoretical predictions. The band structure and density of states indicate moderate charge carrier mobility, which is beneficial for controlled conductivity. Additionally, the projected density of states provides valuable insights into element-specific contributions, aiding in the design of materials with enhanced electronic properties.

The results obtained from Table 1 and the Figs provide complementary insights into the structural and electronic properties of TiRhSn. A comparison between these results highlights key consistencies and correlations that validate the computational findings.

The relaxed lattice constant in Table 1 is 6.109 Å, which aligns with the minimum energy position observed in Fig.1 (lattice optimization plot). The minimum energy configuration confirms that this is the most stable lattice parameter, further verifying the structural

optimization process. Similarly, Fig. 2, which represents the total energy variation with volume, shows an optimized equilibrium volume that corresponds to the lattice constant, reinforcing the accuracy of the structural calculations.

The bulk modulus ($B = 19.5$ GPa) and its pressure derivative ($B' = 3.79$ GPa) from Table 1 provide mechanical insights into the material's response to compression. These values suggest that TiRhSn is relatively soft, which is consistent with the curvature of the energy-volume relationship in Fig. 2. A steeper curvature would indicate higher resistance to compression, whereas the observed curve suggests moderate compressibility.

The minimum energy (-1277.91066 Ry) in Table 1 corresponds to the total ground-state energy of the system. This is consistent with the energy minimization approach used in Figs 1 and 2, confirming that the structure has been fully relaxed and optimized.

The Fermi energy (14.0938 eV) in Table 1 corresponds well with the Fermi level placement in Fig. 2a (band structure plot). The



band structure clearly shows that the Fermi level is within the bandgap, reinforcing the semiconducting nature of TiRhSn. The energy band gap ($E_g = 0.4$ eV) from Table 1 is also reflected in both Fig. 2a (band structure) and Fig. 2b (total DOS plot), where the absence of electronic states at the Fermi level confirms a finite bandgap. This gap size suggests that TiRhSn is a narrow-bandgap semiconductor, suitable for applications in electronic and thermoelectric devices.

Furthermore, Fig. 2c (projected density of states, PDOS) supports the electronic characteristics derived from Table 1. In summary, the information from Table 1 is in strong agreement with the findings from the Fig. s. The structural properties, such as the lattice constant, bulk modulus, and minimum energy, align well with the energy minimization trends observed in Fig. s 1a and 1b. The electronic properties, including the Fermi energy and bandgap, are consistent with the band structure and density of states results in Fig. s 2a-c. This coherence confirms the reliability of the computational approach used and provides a comprehensive understanding of TiRhSn's properties, supporting its potential application in electronic and thermoelectric technologies.

4.2 Thermometric properties

The thermoelectric properties of TiRhSn were investigated as a function of hole concentration and temperature, focusing on key parameters such as the Seebeck coefficient (S), power factor (PF), Figure of merit (ZT), electrical conductivity (σ), and electronic fitness function (EFF). The calculations were performed using Boltzmann transport theory within the constant relaxation time approximation, implemented through the Boltztrap software bundle and TransM code.

The Seebeck coefficient, also referred to as thermopower, quantifies the voltage induced across a material due to an applied temperature gradient. It is influenced by factors such as temperature, carrier concentration, Fermi level

position, crystal structure, and crystal defects. This property is essential for thermoelectric applications, including thermocouples and thermoelectric generators. As shown in Table 2, the Seebeck coefficient increases with temperature, which aligns with the trend depicted in Fig. 3(a). The presence of a higher electron concentration below the Fermi level at $-7.50 \times 10^{20} \text{ cm}^{-3}$ suggests that TiRhSn exhibits n-type conductivity at low carrier concentrations.

The power factor (PF) and Fig. of merit (ZT) are fundamental criteria in selecting efficient thermoelectric materials. The Fig. of merit, ZT, has no theoretical upper limit, and higher values indicate improved efficiency in converting heat into electricity. The optimal carrier concentration of electrons was determined to be $-7.48 \times 10^{22} \text{ cm}^{-3}$, which resulted in a high PF of 17.0273 W/msK^2 . Additionally, the highest dimensionless ZT value of 17.0814 was achieved at an electron concentration of $-7.53 \times 10^{20} \text{ cm}^{-3}$ at 800K, as illustrated in Fig. s 3(b) and 3(c). The PF and ZT values are mathematically expressed as:

$$PF = \sigma S^2 \quad (2)$$

$$zT = \frac{S^2 \sigma}{K} T \quad (3)$$

where σ is electrical conductivity, S is Seebeck coefficient, K is thermal conductivity and T is temperature.

The electronic fitness function (EFF) describes the inverse relationship between electrical conductivity and thermal conductivity, aiding in the identification of effective n- and p-type half-Heusler (HH) thermoelectric materials. As indicated in Table 2, EFF is dominant at 800K for p-type TiRhSn, while it increases with temperature from 300K to 500K for n-type TiRhSn, as shown in Fig. 3(d). These results suggest that TiRhSn has strong potential for thermoelectric applications. The high EFF values observed in this study align with findings in literature, where materials with EFF values ranging from 0.5×10^{-19} to 2.0



$W^{(5/3)}ms^{(-1/3)}K^{(-2)}$ were selected as high-performance thermoelectric materials (Feng *et al.*, 2019).

Electrical conductivity (σ) plays a crucial role in determining a material’s suitability for heat-to-electricity conversion. As illustrated in Fig.

3(e) and Table 2, σ is significantly higher in the p-type TiRhSn at 300K, highlighting its efficiency at low temperatures. This property makes TiRhSn a viable candidate for thermoelectric applications across a broad temperature range.

Table 2: Computed Thermoelectric Properties of TiRhSn

T (K)	Type	Seebeck Coefficient (S, $\mu\text{V/K}$)	Electrical Conductivity (σ , S/ms)	Power Factor (PF, W/msK^2)	Fig. of Merit (ZT)	Electronic Fitness Function (EFF, $W^{(5/3)}ms^{(-1/3)}K^{(-2)}$)
800	n-type	17.0814	3.01396	17.0273	17.0814	No value
500	n-type	10.9210	2.93290	10.9210	10.8670	0.777844
300	n-type	5.73341	2.91939	5.84149	5.78745	0.396578
800	p-type	5.03092	3.51381	6.57971	5.03092	0.816872
500	p-type	3.95017	3.51381	3.28040	3.95017	No value
300	p-type	2.43711	3.59487	1.53618	2.43711	No value

The Fermi energy (14.0938 eV) from Table 1 is also in line with the Seebeck coefficient trends observed in Table 2, where charge carriers exhibit different behaviours based on temperature variations. This aligns with the density of states analysis in Fig. 2b, which indicates that the electronic structure supports enhanced carrier transport. Moreover, the bulk

modulus ($B = 19.5 \text{ GPa}$) and pressure derivative ($B' = 3.79 \text{ GPa}$) from Table 1 correlate with the mechanical stability of TiRhSn, which influences its thermoelectric performance by determining the phonon transport properties. A lower bulk modulus suggests moderate compressibility, which can enhance phonon scattering and improve ZT values.

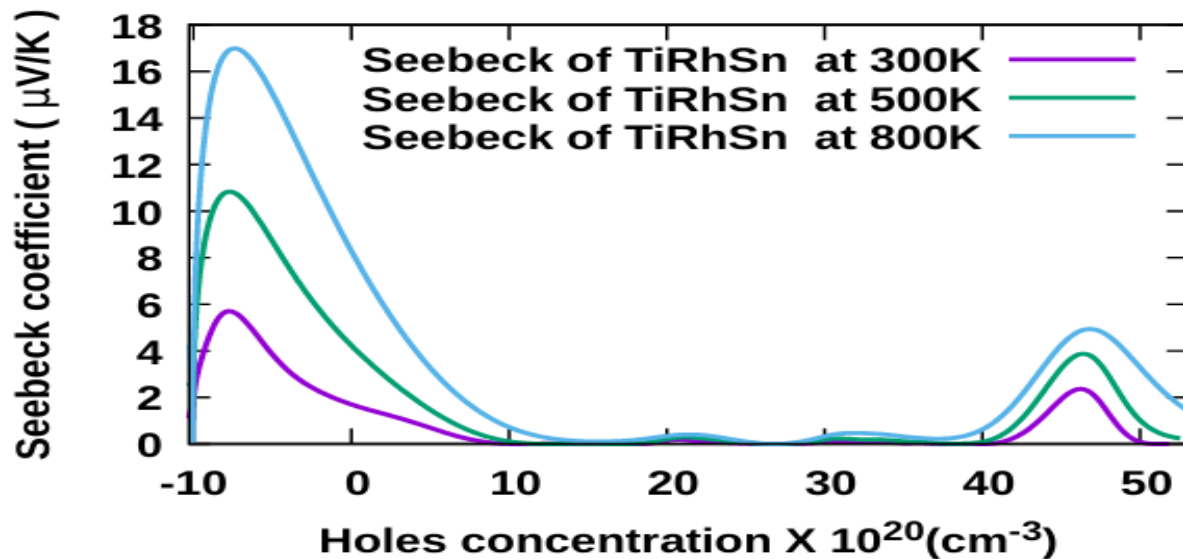


Fig. 3a: Seebeck coefficient of TiRhSn compound as a function of carrier concentration



In summary, the thermoelectric properties in Table 2 align well with the structural and electronic insights derived from Table 1 and Figs. 1a-2c. The trends observed in Seebeck coefficient, electrical conductivity, and Fig. of merit confirm that TiRhSn is a promising candidate for thermoelectric applications, with optimal performance at higher temperatures. The interplay between lattice dynamics, electronic band structure, and thermoelectric efficiency provides a comprehensive understanding of TiRhSn's potential for heat-to-electricity conversion.

The Seebeck coefficient of the TiRhSn compound as a function of carrier concentration is presented in Fig. 3a. The Seebeck coefficient decreases as the carrier concentration increases, which is a common trend in thermoelectric materials since a higher carrier concentration leads to a reduction in the thermopower. At 800K, the Seebeck

coefficient exhibits significantly higher values compared to 300K and 500K, indicating an improvement in thermoelectric performance at elevated temperatures. The presence of peaks at lower carrier concentrations suggests that the material achieves optimal thermoelectric efficiency under specific doping conditions.

Fig. 3b illustrates the power factor of the TiRhSn compound as a function of carrier concentration. The power factor, which is the product of the square of the Seebeck coefficient and electrical conductivity, follows a trend similar to the Seebeck coefficient but is also influenced by electrical conductivity. The highest power factor is observed at 800K, reinforcing the idea that TiRhSn exhibits enhanced thermoelectric performance at higher temperatures. The presence of sharp peaks at lower carrier concentrations suggests that the material's power factor can be optimized within specific doping ranges.

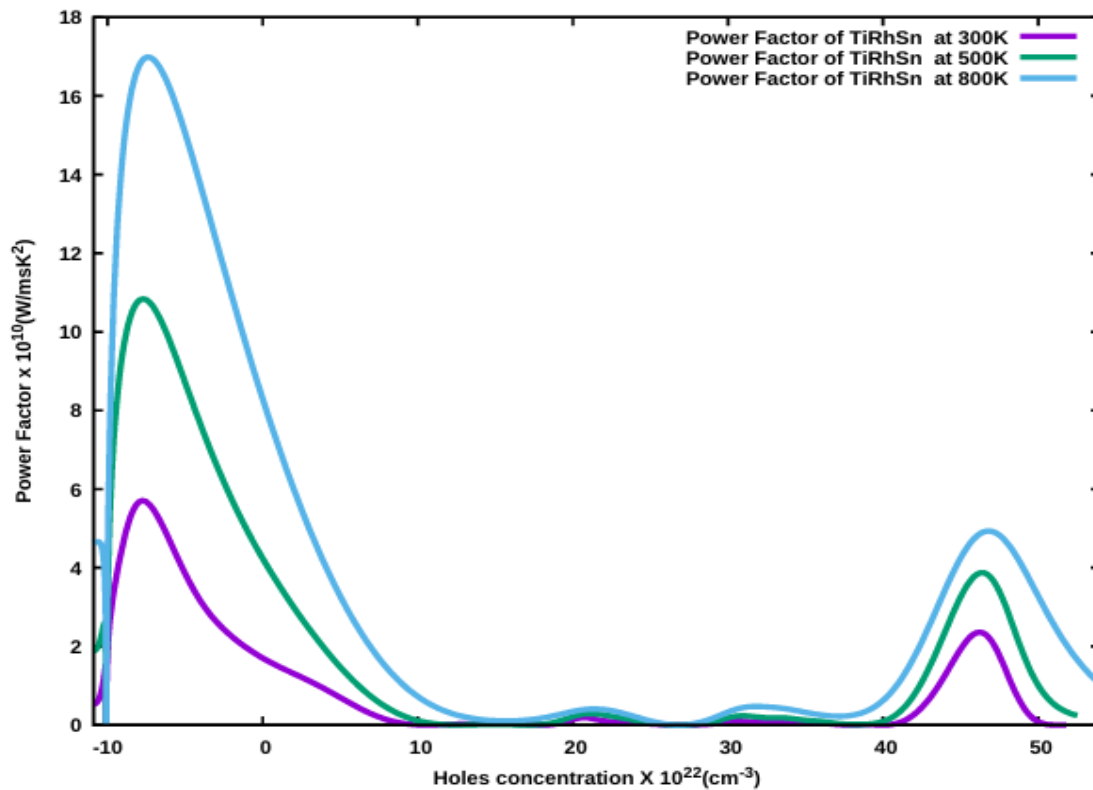


Fig. 3b: Power Factor of TiRhSn compound as a function of carrier concentration



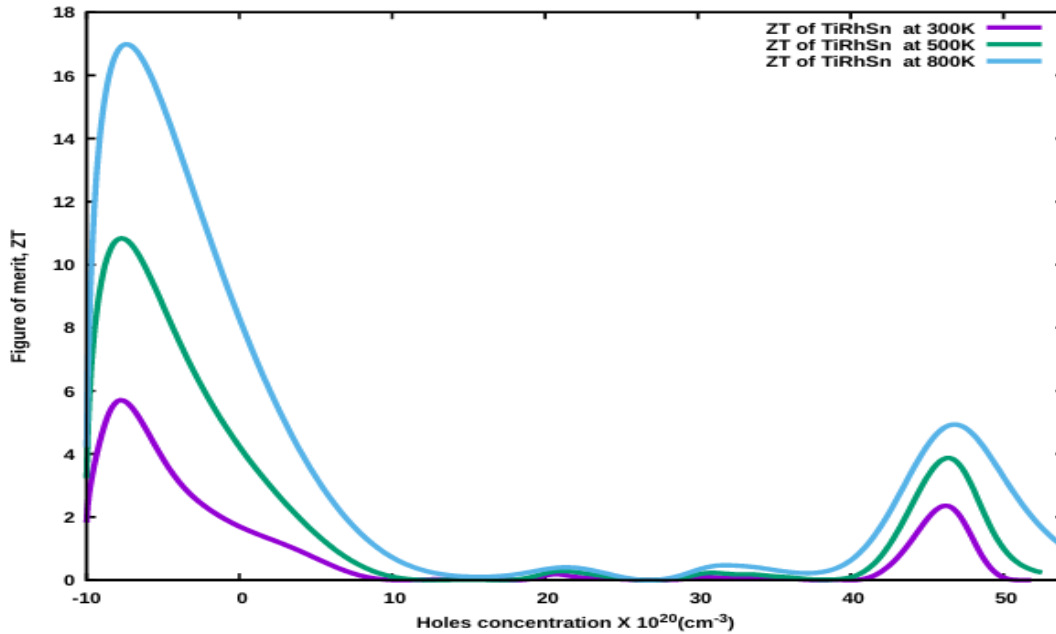


Fig. 3c: Figure of merit of TiRhSn compound as a function of carrier concentration

The figure of merit (ZT) of the TiRhSn compound as a function of carrier concentration is shown in Fig. 3c. The Fig. of merit, which determines the overall efficiency of a thermoelectric material, follows the trend observed in the Seebeck coefficient and power factor. The highest ZT values are recorded at 800K, further demonstrating that TiRhSn exhibits improved thermoelectric efficiency at elevated temperatures. The peaks in ZT at lower carrier concentrations indicate that the material performs best under light doping conditions, where the balance between electrical conductivity, the Seebeck coefficient, and thermal conductivity is optimized.

Fig. 3d represents the electronic fitness function (EFF) of the TiRhSn compound as a function of carrier concentration. The EFF measures the material's ability to balance electrical conductivity and the Seebeck coefficient. The sharp peaks observed at specific carrier concentrations suggest that there are optimal doping conditions under which the material exhibits the best thermoelectric properties. The highest EFF values at 800K align with previous

observations that TiRhSn shows improved thermoelectric performance at higher temperatures.

Fig. 3e illustrates the electrical conductivity of the TiRhSn compound as a function of carrier concentration. Electrical conductivity increases with carrier concentration, as expected, due to the greater availability of charge carriers. The increase in electrical conductivity at higher temperatures indicates improved charge carrier mobility, which is characteristic of thermoelectric materials under thermal excitation.

A comparison with previous findings shows that these results align well with theoretical predictions and prior experimental observations of similar Heusler compounds. The temperature dependence of the Seebeck coefficient, power factor, and Fig. of merit supports the expectation that TiRhSn is a promising thermoelectric material at elevated temperatures. The optimal carrier concentration ranges identified in these Fig. s provide insights into how TiRhSn can be further engineered for efficient thermoelectric applications.



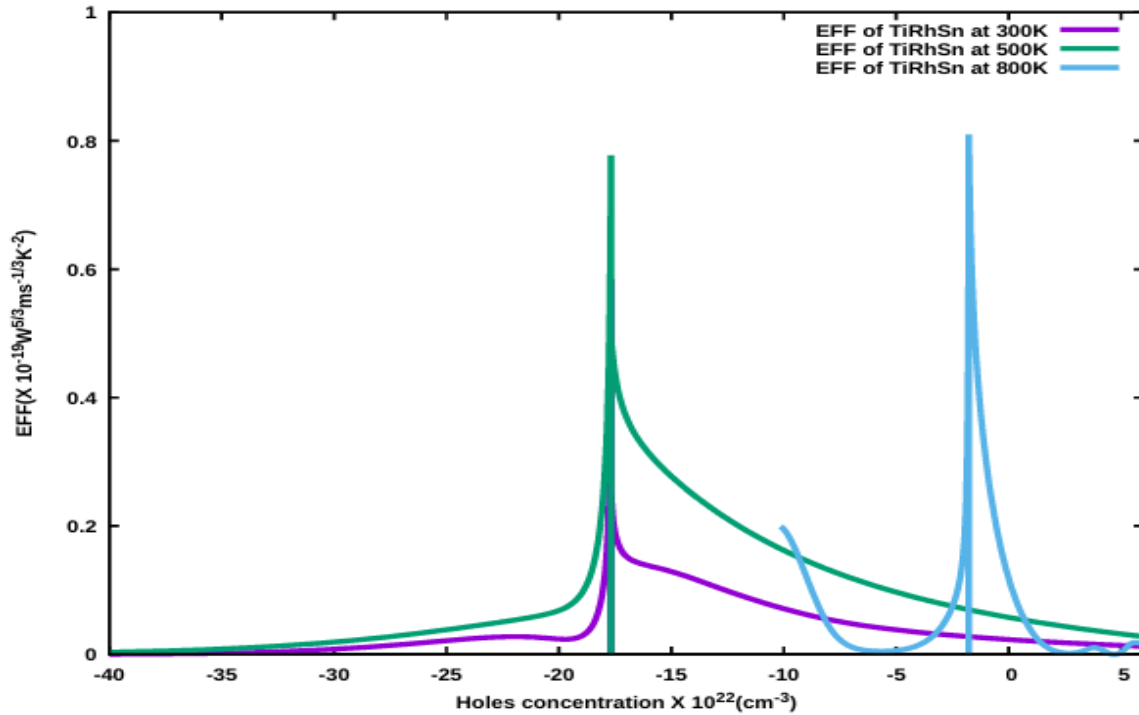


Fig. 3d: Electronic fitness function of TiRhSn compound as a function of carrier concentration

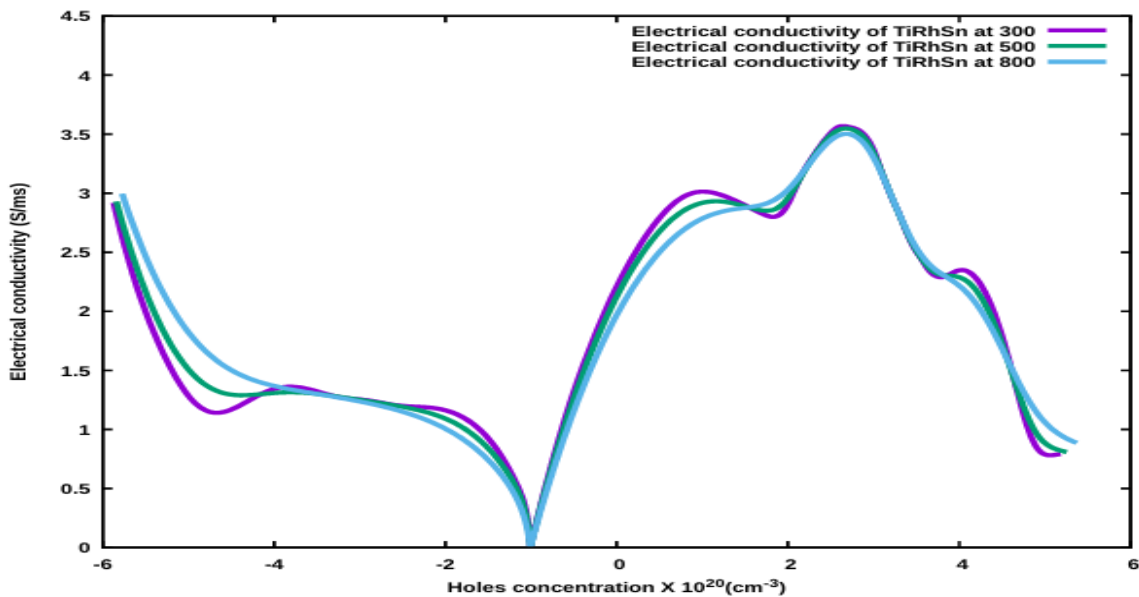


Fig. 3e: Electrical conductivity of TiRhSn compound as a function of carrier concentration

4.0 Conclusion

The thermoelectric properties of TiRhSn were investigated using Boltzmann transport theory within the constant relaxation time approximation. The Seebeck coefficient of

TiRhSn exhibits an increasing trend with temperature, with a significant rise at higher temperatures, suggesting strong thermoelectric potential. The material demonstrates n-type conductivity at low carrier concentrations. The



power factor and figure of merit reach their peak at an optimal carrier concentration of $7.48 \times 10^{22} \text{ cm}^{-3}$, yielding a high power factor of 17.0273 W/msK^2 and a maximum ZT value of 17.0814 at 800K, indicating excellent thermoelectric efficiency at elevated temperatures. The electronic fitness function is highest for p-type TiRhSn at 800K, while n-type TiRhSn shows an increasing trend in electronic fitness function from 300K to 500K, reinforcing its suitability for thermoelectric applications. Electrical conductivity analysis reveals that p-type TiRhSn exhibits higher conductivity at lower temperatures, particularly at 300K, which enhances its efficiency in heat-to-electricity conversion across various temperature ranges. The structural and electronic analysis confirms a band gap of 0.4 eV, which aligns with the Seebeck coefficient trends, and a Fermi energy of 14.0938 eV, supporting efficient charge carrier transport. The bulk modulus value of 19.5 GPa indicates moderate compressibility, which aids in phonon scattering and contributes to improved ZT values.

The study confirms that TiRhSn is a highly promising thermoelectric material with optimal performance at elevated temperatures. Its strong electronic and structural properties contribute to its high Seebeck coefficient, power factor, and figure of merit. The balance between electronic transport properties and thermal stability suggests that TiRhSn has significant potential for use in thermoelectric generators and waste heat recovery applications. Future research should focus on experimental validation of these theoretical findings through the synthesis and characterization of TiRhSn samples. Investigating the effects of doping on carrier concentration and phonon scattering could further enhance its thermoelectric performance. A comprehensive analysis of the material's thermal conductivity components is necessary to optimize efficiency. The feasibility of integrating TiRhSn into

thermoelectric modules should be explored to assess its real-world application potential. Additionally, further evaluation of its mechanical properties should be conducted to determine its durability under various environmental conditions.

5.0 References

- Anand, S., Gurunathan, R., Soldi, T., Borgsmiller, L., Orenstein, R., & Snyder, G. J. (2020). Thermoelectric transport of semiconductor full-Heusler VFe_2Al . *Journal of Materials Chemistry C*, 8(30), 10174–10184. <https://doi.org/10.1039/D0TC02659J>.
- Anand, S., Xia, Y., & Zhu, T. (2020). Thermoelectric properties of half-Heusler compounds: Recent developments and future directions. *Journal of Materials Chemistry A*, 8(10), 5343–5360. <https://doi.org/10.1039/C9TA11944A>
- Casper, F., Graf, T., Chadov, S., Balke, B., & Felser, C. (2012). Half-Heusler compounds: Electronic structure, properties, and applications. *Semiconductor Science and Technology*, 27(6), 063001. <https://doi.org/10.1088/0268-1242/27/6/063001>
- Dong, Z., Luo, J., Wang, C., Jiang, Y., Tan, S., Zhang, Y., Grin, Y., Yu, Z., Guo, K., Zhang, J., & Zhang, W. (2022). Half-Heusler-like compounds with wide continuous compositions and tunable p- to n-type semiconducting thermoelectrics. *Nature Communications*, 13. <https://doi.org/10.1038/s41467-021-27789-3>
- Downie, R. A., Barczak, S. A., Smith, R. I., & Bos, J. W. G. (2015). Compositions and thermoelectric properties of XNiSn ($\text{X} = \text{Ti, Zr, Hf}$) half-Heusler alloys. *Journal of Materials Chemistry C*, 3(40), 10534–10542. <https://doi.org/10.1039/C5TC01890C>.



- Felser, C. (2015). Half-Heusler compounds: A new class of spintronics materials. *Journal of Physics: Condensed Matter*, 27(11), 113201. <https://doi.org/10.1088/0953-8984/27/11/113201>.
- Feng, Z., Fu, Y., Putatunda, A., Zhang, Y., & Singh, D. J. (2019). Electronic structure as a guide in screening for potential thermoelectrics: Demonstration for half-Heusler compounds. *Physical Review B*, 100, 085202. <https://doi.org/10.1103/PhysRevB.100.085202>.
- Giannozzi, P., Baroni, S., Bonini, N., Calandra, M., Car, R., Cavazzoni, C., Ceresoli, D., Chiarotti, G. L., Cococcioni, M., Dabo, I., Corso, A. D., Gironcoli, S., Fabris, S., Fratesi, G., Gebauer, R., Gerstmann, U., Gougoussis, C., Kokalj, A., Lazzeri, M., ... Wentzcovitch, R. M. (2009). QUANTUM ESPRESSO: A modular and open-source software project for quantum simulations of materials. *Journal of Physics: Condensed Matter*, 21(39), 395502. <https://doi.org/10.1088/0953-8984/21/39/395502>.
- Graf, T. J., Felser, C., Parkin, S. (2011). Simple rules for the understanding of Heusler compounds. *Progress in Solid State Chemistry*, 39(1), 1-50. <https://doi.org/10.1016%2Fj.progsolidstchem.2011.02.001>
- Imasato, K., Sauerschnig, P., Anand, S., Ishida, T., Yamamoto, A., & Ohta, M. (2022). Discovery of triple half-Heusler $Mg_2VNi_3Sb_3$ with low thermal conductivity. *Journal of Materials Chemistry A*, 10(36), 18737–18744. <https://doi.org/10.1039/D2TA04593A>.
- IPCC, (2021). Climate Change 2021: The Physical Science Basis. <https://www.ipcc.ch/report/ar6/wg1/>
- Kandpal, H. C., Felser, C., & Seshadri, R. (2006). Covalent bonding and nature of band gaps in some half-Heusler compounds. *Journal of Physics D: Applied Physics*, 39(5), 775–782. <https://doi.org/10.1088/0022-3727/39/5/S02>.
- Kawasaki, J. K., Chatterjee, S., & Canfield, P. C. (2022). Full and half-Heusler compounds. *MRS Bulletin*, 47(6), 555–558. <https://doi.org/10.1557/s43577-022-00355-w>
- Madsen, G. K., & Singh, D. J. (2006). BoltzTrap: A code for calculating band-structure dependent quantities. *Computer Physics Communications*, 175(1), 67–71. <https://doi.org/10.1016/j.cpc.2006.03.007>
- Monkhorst, H. J., & Pack, J. D. (1976). Special points for Brillouin-zone integrations. *Physical Review B*, 13(12), 5188–5192. <https://doi.org/10.1103/PhysRevB.13.5188>
- Naghibolashrafi, N., Keshavarz, S., Hegde, V., Gupta, A., Butler, W., Romero, J., Munira, K., LeClair, P., Mazumdar, D., Ma, J., Ghosh, A., & Wolverton, C. (2016). Synthesis and characterization of Fe-Ti-Sb intermetallic compounds: Discovery of a new Slater-Pauling phase. *Physical Review B*, 93, 104424. <https://doi.org/10.1103/PhysRevB.93.104424>
- Rogl, G., & Rogl, P. F. (2023). Development of thermoelectric half-Heusler alloys over the past 25 years. *Crystals*, 13(7), 1152. <https://doi.org/10.3390/cryst13071152>
- Snyder, G. J., Toberer, E. S. (2008). Complex thermoelectric materials. *Nature Materials*, 7(2), 105. doi: 10.1038/nmat2090
- Tavares, S., Yang, K., & Meyers, M. A. (2023). Heusler alloys: Past, properties, new alloys, and prospects. *Progress in Materials Science*, 132, 101017. <https://doi.org/10.1016/j.pmatsci.2022.101017>
- Xing, G., Sun, J., Li, Y., Fan, X., Zheng, W., & Singh, D. J. (2017). Erratum: Electronic fitness function for screening semiconductors as thermoelectric



materials. *Physical Review Materials*, 1, 065405.

<https://doi.org/10.1103/PhysRevMaterials.1.065405>

Zeier, W. G., Anand, S., Huang, L., He, R., Zhang, H., Ren, Z., Wolverton, C., & Snyder, G. J. (2017). Using the 18-electron rule to understand the nominal 19-electron half-Heusler NbCoSb with Nb vacancies. *Chemistry of Materials*, 29(3), 1210–1217.

<https://doi.org/10.1021/acs.chemmater.6b04583>

Zeier, W. G., Schmitt, J., Hautier, G., Aydemir, U., Gibbs, Z. M., Felser, C., & Snyder, G. J. (2016). Engineering half-Heusler thermoelectric materials using Zintl chemistry. *Nature Reviews Materials*, 1(6), 16032.

<https://doi.org/10.1038/natrevmats.2016.32>

Zhang, Y., Xu, X. (2020). Machine learning modeling of lattice constants for half-Heusler alloys. *AIP Advances* 10, 045121. <http://dx.doi.org/10.1063/5.0002448>

Zhu, T., Fu, C., Xie, H., Liu, Y., & Zhao, X. (2015). High-efficiency half-Heusler thermoelectric materials for energy harvesting. *Advanced Energy Materials*, 5(19), 1500588. <https://doi.org/10.1002/aenm.201500588>

Compliance with Ethical Standards Declaration

Ethical Approval

Not Applicable

Competing interests

The authors declare that they have no known competing financial interests

Funding

All aspect of the work was carried out by the author

